Received: 29 November 2018 | Revised: 7 July 2019 | Accepted: 29 August 2019

DOI: 10.1002/we.2424

RESEARCH ARTICLE

WILEY

Validation and uncertainty quantification of metocean models for assessing hurricane risk

Chi Qiao | Andrew T. Myers | Sanjay R. Arwade

Department of Civil & Environmental Engineering, University of Massachusetts, Amherst, MA, USA

Correspondence
A. T. Myers, Department of Civil & Environmental Engineering, Northeastern University, Boston, MA, USA.
Email: atm@neu.edu

Funding information
National Science Foundation, Grant/Award Numbers: CMMI-1234560 and CMMI-1552559; Northeastern University; Massachusetts Clean Energy Center

Abstract

A reliable metocean model, with its uncertainty quantified and its accuracy validated for conditions appropriate to assessing risk, is essential to understand the risk posed by hurricanes to offshore infrastructure such as offshore wind turbines. In this paper, three metocean models are considered, with the seastate predicted using the commercial software Mike 21, and the meteorological forcing defined by three conditions. The three conditions include (1) reanalysis data within and surrounding the hurricane, (2) predictions from the empirical Holland model within the hurricane and reanalysis data surrounding the hurricane, and (3) predictions from the empirical Holland model within the hurricane and wind-free conditions surrounding the hurricane. The accuracy of the first metocean model is validated with (1) measurements of wind speed, wave height, wave period, and storm surge during 23 historical hurricanes from 1999 to 2012 and (2) a comparison to hindcast data from WaveWatch III, another numerical metocean model. The prediction performance of the second and third metocean models is then compared with that of the first to evaluate the impact of meteorological conditions on model predictions, as the third metocean model is necessary for risk analysis, where reanalysis data of meteorological conditions is not available. This study shows that the inconsistency between the modeling of meteorological conditions for risk assessment and for validation is influential for hurricanes with low maximum wind speeds, when model predictions are significantly better if the meteorological conditions surrounding the hurricane wind field are included. This study also shows that this inconsistency is effectively diminished when considering only events with high maximum wind speeds. Since high wind speeds are what is relevant to risk assessments, the third metocean model can be reasonably used to assess hurricane risk. Finally, the uncertainties, biases, and correlations of uncertainties in the model predictions for wind speed, wave height, wave period, and storm surge are quantified for the third metocean model, and a numerical example is constructed to illustrate the impact of including uncertainty on the assessment of risk to offshore infrastructure during hurricanes. The example demonstrates how uncertainty and correlation of uncertainty influence the size and shape of a 50-year environmental contour of wind speed and wave height.

KEYWORDS

numerical model validation, offshore hurricane multi-hazard, risk analysis, uncertainty quantification

1 | INTRODUCTION

The U.S. Atlantic coast is a natural location to install offshore wind turbines due to its rich wind resource, relatively shallow water, and proximity to population centers. Offshore infrastructure installed in this region is exposed to multiple hurricane-induced hazards, such as wind, wave, and storm surge. The correlation among these hazards, plus the short historical record of hurricanes (~30 years for detailed records) and the relative paucity of measurements of offshore conditions during hurricanes, make the design and risk assessment of offshore infrastructure along the U.S. Atlantic coast a challenging endeavor.

One approach to overcome these challenges is to use numerical models to simulate metocean conditions for a catalog of synthetic hurricanes that more completely represents potential hurricane variability by simulating thousands of years of potential hurricane activity.[1-3] Before a numerical metocean model is applied to hurricane risk analysis, several aspects of the model should be understood, and three of these aspects are studied here. The first aspect is the accuracy of the model, that is, the governing equations of the underlying physics to be modeled. A common approach to measure accuracy is to validate the model predictions against measurements during historical hurricanes.[4-6] The accuracy of the model, however, must be weighed against the efficiency of the model, as risk assessments typically require the simulation of thousands of hurricanes. The second aspect is the degree to which the model predictions differ when the meteorological conditions in the model are based on a simplified empirical model, such as the Holland model,[7] and when they are based on reanalysis data. This distinction is important as meteorological conditions from reanalysis data are often used for model validation, while empirical models are often used for assessing risk, which usually considers synthetic hurricanes for which reanalysis data is not available. The difference between these meteorological conditions arises from simplifications in the empirical model compared with reanalysis data and the inability of empirical models like the Holland model to represent meteorological conditions surrounding the hurricane. The impact of this difference on the performance of metocean models is evaluated by several studies for the Gulf of Mexico,[8,9] but has not been well assessed for the U.S. Atlantic coast region. The third and final aspect considered here is quantification of the overall prediction uncertainty, which includes contributions from the seastate prediction model and from the meteorological forcing (induced either by imperfections of the numerical model in a reanalysis study or by simplification of the Holland model), and how this uncertainty affects the assessment of hurricane risk.

In this paper, a numerical model is implemented for predicting seastates during hurricanes along the U.S. Atlantic coast. This model is implemented by the authors within the commercial program Mike 21. In order to evaluate the three aspects mentioned above, three metocean models are considered by using different meteorological conditions (i.e., the wind and pressure fields) as input to the seastate prediction model: (1) the Mike 21 model driven by reanalysis data from the Climate Forecast System Reanalysis (CFSR) study[10] within and surrounding the hurricane (named herein as the CFSR/Mike 21 model), (2) the Mike 21 model driven by predictions from the empirical Holland model[7] within the hurricane and CFSR data surrounding the hurricane (named herein as the Hybrid/Mike 21 model), and (3) the Mike 21 model driven by predictions from the Holland model within the hurricane and wind-free conditions surrounding the hurricane (named herein as the Holland/Mike 21 model). Predictions of the sustained wind speed V, the significant wave height H_s, the peak spectral period T_p, and the storm surge η are compared with corresponding buoy measurements during a set of 23 historical hurricanes at 107 locations. The prediction performance of the CFSR/Mike 21 model is compared with the hindcast data from another numerical metocean model, WaveWatch III (WW3),[11] which uses the same meteorological forcing, for the purpose of model validation. The Hybrid/Mike 21 model is compared with the CFSR/Mike 21 model to assess the influence of modeling meteorological conditions using the simple empirical Holland model compared with reanalysis data. The Holland/Mike 21 model is compared with the Hybrid/Mike 21 model to evaluate the impact of the meteorological condition surrounding the hurricane on metocean predictions. Since prediction uncertainty affects the assessment of risk, and reanalysis data is not available for synthetic hurricanes, which are commonly used in the assessment of risk, the Holland/Mike 21 model is also used to quantify the bias and uncertainty of the model. It is important to note that this paper is not intended to develop a better metocean prediction model, but rather to quantify the uncertainty of practical models and evaluate its impact on risk analysis.

This paper first summarizes the information of the meteorological and seastate prediction models involved in this study in Section 2 and then provides details on the validation of the CFSR/Mike 21 model implemented here in Section 3, including specification of the historical hurricanes and metocean measurements used for validation. In Section 4, the impact of the meteorological forcing on the prediction performance of the Mike 21 model is discussed. In Section 5, biases and uncertainties of the Holland/Mike 21 model are quantified, followed by a numerical example showing the influence of uncertainty on the assessment of offshore hurricane risk. Finally in Section 6, the conclusions of this study are summarized.

2 | MODEL BACKGROUND

This paper compares the prediction performance of three metocean models with the seastate predicted by the Mike 21 model and the meteorological conditions defined by three combinations of meteorological models. The three meteorological conditions are defined separately for locations within the hurricane (i.e., within $2R_{max}$, where R_{max} is the radius of maximum winds) and surrounding the hurricane (i.e., outside $3R_{max}$), see Table 1. Within the hurricane, two types of meteorological forcing are considered: those from CFSR and those from the empirical Holland model.

TABLE 1 Three combinations of meteorological models used to evaluate the impact of meteorological forcing on seastates predicted by the Mike 21 model

Name	Model within hurricane	Model surrounding hurricane
CFSR	CFSR	CFSR
Hybrid	Holland	CFSR
Holland	Holland	None

Surrounding the hurricane, two types of meteorological forcing are considered: those from CFSR and wind-free conditions (i.e., the field surrounding the hurricane is modeled as having zero wind speed and standard atmospheric pressure). More details on the meteorological conditions are provided in Section 2.1.

In addition to the Mike 21 model, another seastate prediction model, WW3, is considered for comparison. The WW3 model only provides predictions of H_s and T_p, while the Mike 21 model provides predictions of H_s, T_p, and η. More details on the two seastate prediction models are provided in Section 2.2.

2.1 | Meteorological conditions

This section provides details on the three combinations (CFSR, Holland, and Hybrid) of meteorological models considered in this paper to define the meteorological forcing for seastate prediction models. CFSR is implemented by other researchers,[10] while the Holland and Hybrid models are implemented by the authors.

2.1.1 | CFSR

The CFSR wind (at 10 m elevation) and pressure (at sea level) fields are generated from a global-scale reanalysis using the CFS[12] (Climate Forecast System), which is implemented by the National Centers for Environmental Prediction (NCEP). This reanalysis assimilates data from satellite radiances and all available conventional observations (e.g., buoy measurements and ship observations) at 6-hour intervals and uses a coupled atmosphere-ocean-land model for making hourly forecasts.

The reanalysis data used in this study[13,14] is obtained from two separate versions of the CFS. Both versions provide information at 1-hour intervals and the older one, which covers the time period 1979-2011, has a slightly coarser spatial resolution of 0.31° than the newer one, which covers the time period 2011-2016 with a spatial resolution of 0.21°. The information from both versions is interpolated here to the same resolution of 0.054° using cubic interpolation. Cubic interpolation is preferred over linear interpolation to alleviate the spatial averaging effect of this mesoscale model. However, CFSR is not sufficient to capture the full characteristics of the hurricane wind field.[15] For a more accurate wave hindcast during hurricanes, a common approach is to overlay hurricane forcing provided by either a proven mesoscale model (e.g., the WRF model[16]) or hurricane snapshots provided by National Hurricane Research Division[17,18]; however, this approach is not possible when assessing risk using a catalog of synthetic hurricanes which defines hurricanes in terms of several parameters, as is common in practice. The CFSR data is used here because it is readily available, and more importantly, because it is useful to compare the accuracy of metocean responses driven by CFSR with responses driven by empirical meteorological models, to give practitioners a sense of the accuracy expected when using the empirical models.

2.1.2 | Holland model

The Holland model[7] is a widely-used, empirical model[19-21] that estimates the meteorological conditions of hurricanes based on seven hurricane parameters: the position of the hurricane eye (i.e., latitude and longitude), the central pressure P_c, the translation speed V_{tr}, the heading direction, the radius of maximum winds R_{max}, and the Holland B parameter. The model describes the hurricane pressure field P as a function of radial distance from the hurricane eye r,

$$P(r) = P_c + (P_n - P_c)\exp\left[-\left(\frac{R_{max}}{r}\right)^B\right] \tag{1}$$

where P_n is the peripheral pressure. Combining this pressure field with the gradient wind equation and adding the hurricane translation speed, the mean wind speed at gradient height V_g is expressed as,

$$V_g(r,\theta) = \left[\frac{B}{\rho}\left(\frac{R_{max}}{r}\right)^B (P_n - P_c)\exp\left[-\left(\frac{R_{max}}{r}\right)^B\right] + \frac{(V_{tr}\sin\theta - rf_c)^2}{4}\right]^{0.5} + \frac{V_{tr}\sin\theta - rf_c}{2} \tag{2}$$

where ρ is air density, θ is the angle measured clockwise starting from the hurricane heading direction, and f_c is the Coriolis parameter. A constant factor of 0.71 is applied to convert the wind speed from gradient height to 10 m when comparing with measurements[22] and as input to the Mike 21 model. Note that Eq. 2 includes the asymmetries of the hurricane wind field, which is proposed by Georgiou et. al[23] as an early improvement to the original Holland model. Several more recent studies[24-26] have further improved the Holland model.

The seven input parameters required by the Holland model are obtained from multiple sources for the historical hurricanes considered in this study. Hurricane eye position is taken from the International Best Track Archive for Climate Stewardship (IBTrACS) database,[27] which provides historical hurricane track data at 6-hour intervals. The translation speed V_{tr} and heading direction are derived from the eye position in the IBTrACS database. P_c and R_{max} are obtained from the H*wind database,[28] which provides one-minute maximum wind reanalysis data at 10 m height for hurricane wind fields at 6-hour intervals and a spatial resolution of 0.054°. The Holland B parameter represents the rate of decay of the wind field of the hurricane with respect to position relative to the eye, and several approaches have been proposed to calculate this parameter.[29,30] In this study, a method similar to that proposed by Vickery and Wadhera,[30] wherein the B parameter is selected by minimizing the root mean square error between the wind field of the Holland model and the H*wind reanalysis over the range of 0.5 R_{max} to 1.5 R_{max}, is adopted. Since both the wind measurements (see Section 3.2) and the H*wind used to determine the parameters for the Holland model are near the sea surface level (within 50 m), the simple conversion factor of 0.71 from gradient height to 10 m does not affect the results here. A factor of 0.90 is used to convert the H*wind reanalysis from one-minute maximum wind to mean wind.[31]

For many hurricanes in this study, P_c, R_{max} and the Holland B parameter need to be specified for times in addition to those provided by H*Wind. In these cases, P_c is taken from IBTrACS database, R_{max} is estimated using the equation proposed by Vickery and Wadhera,[30]

$$\ln(R_{max}) = 3.421 - 4.600 \times 10^{-5}(P_n - P_c)^2 + 0.00062\psi^2 \tag{3}$$

where ψ is latitude, and the Holland B parameter is estimated using the following equation,[7]

$$B = \frac{\rho e V_{max}^2}{P_n - P_c} \tag{4}$$

where e is the base of the natural logarithm and V_{max} is the maximum gradient wind speed provided by the IBTrACS database. Note that Eq. 3 represents the statistical mean of the sample and that the H*wind reanalysis has significant variation about this mean. However, since the results compared in this paper (see Section 3) are within the period provided by H*wind, the impact of this error is minor. The seven hurricane parameters are linearly interpolated to 1-hour intervals to provide a smoother transition of the meteorological conditions for use as inputs to the Mike 21 model.

2.1.3 | Hybrid model

The Holland model does not include any information on the meteorological conditions surrounding the hurricane. Metocean conditions at a particular location are influenced by the meteorological conditions both within and surrounding the hurricane, and it is not clear the extent to which the surrounding conditions influence the prediction of metocean conditions at locations within the hurricane. To examine this question, a hybrid model, with the Holland model defining conditions within the hurricane and CFSR defining conditions surrounding the hurricane, is considered in this study. The specific hybrid model used here is similar to the one proposed by Tanemoto and Ishihara,[32] and the hybrid wind field is expressed as,

$$V_{hybrid} = W \cdot V_{Holland} + (1 - W) \cdot V_{CFSR} \tag{5}$$

where W is a weighting function, which is defined here as,

$$W = \begin{cases} 1 & r \le 2R_{max} \\ \frac{1}{2}\left[\cos\left(\frac{r - 2R_{max}}{R_{max}}\pi\right) + 1\right] & 2R_{max} < r < 3R_{max} \\ 0 & r \ge 3R_{max} \end{cases} \tag{6}$$

and the transition range between $2R_{max}$ and $3R_{max}$ is determined from the prediction performance of the Holland/Mike 21 model (see Section 4). The hybrid pressure field is calculated in a similar manner following Eq. 5.

2.2 | Seastate prediction models

This section provides details on the Mike 21 model implemented by the authors, and the WaveWatch III (WW3) model implemented by NCEP.[33] The WW3 model is selected for comparison with the Mike 21 model because it is a widely-studied model with a similar resolution over the model domain and because the 30-year hindcast data based on this model is publicly available.

2.2.1 | Mike 21

The commercial program Mike 21 is a coastal model that includes separate modules for multiple phenomena. In this study, two coupled modules, Mike 21 HD and Mike 21 SW, are used to predict metocean conditions during hurricanes. Mike 21 HD is the hydrodynamic module and the physics of this module is based on the depth-integrated, incompressible, Reynolds-averaged Navier-Stokes equations.[34] Mike 21 SW is the spectral wave module which simulates the growth, propagation, and decay of wind-generated waves and swells based on a wave action conservation equation.[35] These two modules are coupled in a way that wave radiation from the SW module is included in the HD module for flow calculations, and water level and current from the HD module are included in the SW module for wave calculations. Both modules take mean wind speed at 10 m height as input.

The domain of the Mike 21 HD/SW model implemented here includes the majority of the U.S. Atlantic coast, see Figure 1(a). The domain is extended southward beyond the Atlantic coast to include regions where the propagation of swells may contribute significantly to the metocean conditions along the Atlantic coast. The spatial resolution of the non-structured mesh within the model domain is approximately linear to the water depth, varying between 20 km for deep water areas and 5 km for shallow water areas, and totaling ~66,000 triangular elements, see Figure 1(b). Such resolution is sufficient for modeling metocean response in the offshore area[36,37] and meanwhile ensuring computational efficiency for thousands of synthetic hurricane simulations. The bathymetry in the model is linearly interpolated from the Global Relief Model[38] for most of the model domain and the Coastal Relief Model[39] for the portions of the domain with shallow water. In the HD module, sea bed resistance is modeled with a constant Manning number of 32 $m^{1/3}/s$ for the entire domain.[40] Wind friction is modeled using the drag coefficient proposed by Wu.[41] Tide levels during historical hurricanes are specified along the open boundary of the HD module using the DHI Global Tide Model.[42] In the SW module, wave direction is discretized into 36 bins, each with an angle of 10°, and frequency is discretized into 40 bins logarithmically between 0.03 Hz and 1.42 Hz. The dissipation of energy by depth-induced breaking waves is modeled following the formulation by Battjes and Janssen[43] and therefore the H_s values predicted by the model are influenced by breaking waves. Bottom friction is modeled using a constant Nikuradse roughness[44] of 0.04 m for the entire model domain. The equation proposed by Bidlot et al.[45] is used to describe the dissipation of energy due to white capping. The model boundaries in the SW module are the same as those in the HD module, see Figure 1(a), however, for the SW module, a lateral boundary is applied, meaning that the effect of waves propagating from outside the boundary is neglected.

2.2.2 | WaveWatch III

WW3 is a wave model developed by NCEP.[11] The model predicts metocean conditions considering the actions of wind, bottom friction, and breaking waves. The implementation of the model considered here[33] has a domain spanning the entire globe, with three levels of nested grid resolution: a global grid with 0.50° resolution, an intermediate grid with 0.17° resolution covering the area between ~200 km and ~500 km from shore, and a nearshore grid with 0.067° resolution covering the area within ~100 km from shore.[46] Note that the 0.067° resolution of the nearshore grid is close to the resolution of the Mike 21 model in the same area, and most of the buoy measurements for validation are within this area.

Hindcast data from Version 2.22 of WaveWatch III,[33] which does not include any data assimilation, is used in this study. This version covers the time period 1979-2015 and provides information at 3-hour intervals. The data with a nested grid resolution of 0.067° and 0.17° is only available since 2005.

3 | MODEL VALIDATION

All models considered in this study are compared for the same set of historical hurricanes and corresponding measurements. The prediction error is expressed in terms of the logarithmic error,

$$\varepsilon_x = \ln\hat{x} - \ln x \tag{7}$$

where x is the measurement and $\hat{x}$ is the corresponding prediction. As such, a positive prediction error indicates overestimation. The overall prediction performance is evaluated using the standard deviation of the considered prediction errors, expressed as,

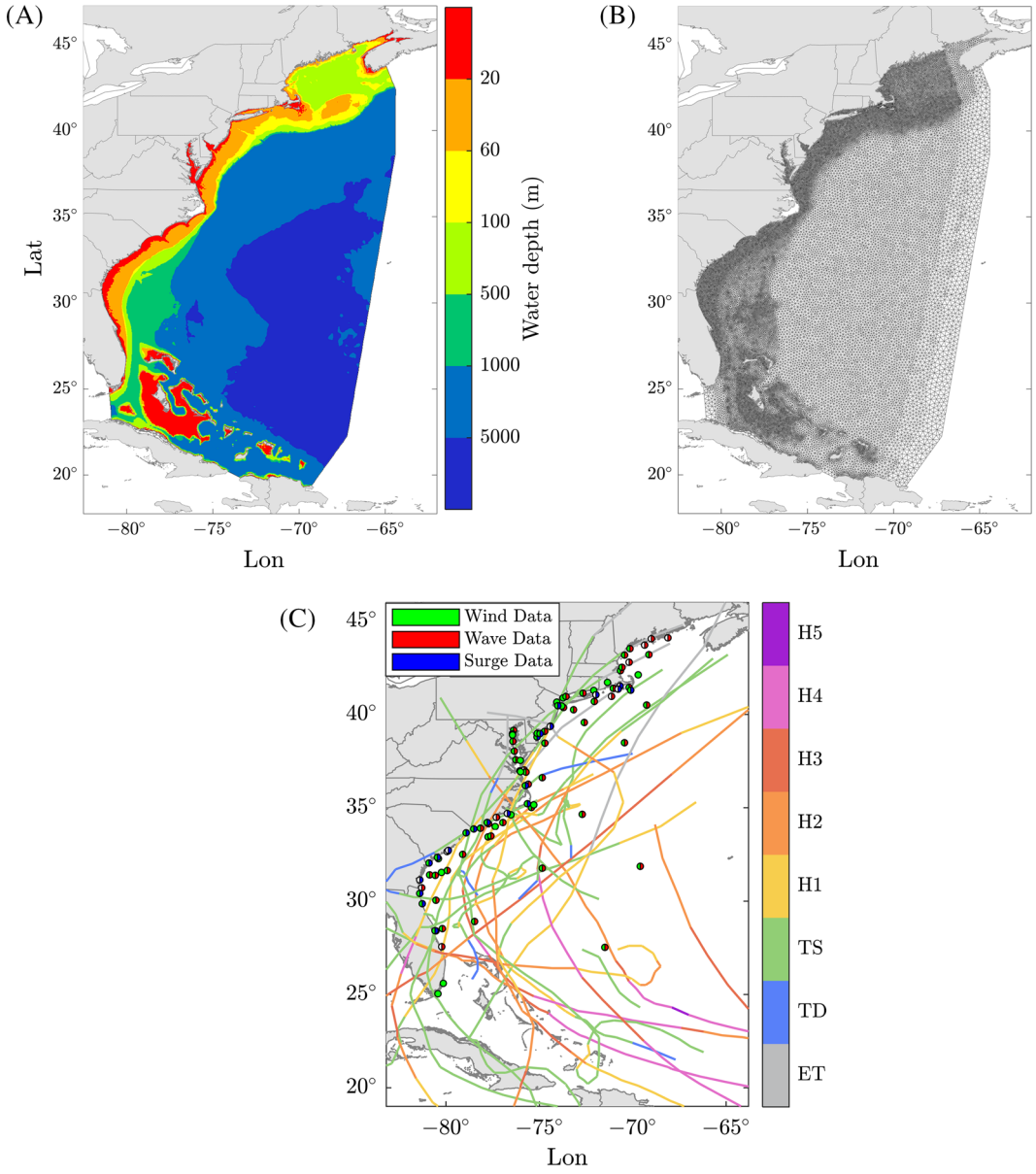

FIGURE 1 The Mike 21 model domain shown with (a) a contour plot of bathymetry, (b) the mesh, and (c) the locations of offshore buoys and what they measured (wind, wave, or storm surge), superimposed with the paths of the 23 historical hurricanes considered here, with the color of the path showing hurricane intensity per the Saffir-Simpson scale (TS: tropical storm, TD: tropical depression, ET: extra-tropical cyclone)

$$\sigma_{\varepsilon_x} = \sqrt{\frac{1}{n}\sum_{i=1}^{n}\left(\varepsilon_{x,i} - \bar{\varepsilon}_x\right)^2} \tag{8}$$

where n is the number of comparisons between prediction and measurement. To provide some context for the meaning of the numerical value of ε_x, it is noted that the percentage values corresponding to ε_x are asymmetric, with a value of ε_x equal to ±0.5 corresponding to 40% overestimation and 65% underestimation of the prediction result compared with the measurement, and a value of ε_x equal to ±0.25 corresponding to 22% overestimation and 28% underestimation. Logarithmic error is widely used in Earthquake Engineering, and this metric is preferred here over the bias error (i.e., $\varepsilon_x = \hat{x} - x$) because its variance shows less dependency on the prediction (see Section 5.1).

For the four types of metocean measurements considered in this study, the maximum values of sustained wind speed V, significant wave height H_s, and storm surge η, and the values of peak spectral period T_p corresponding to the maximum H_s are compared. As such, the synchronization in time both between hazards and between prediction and measurement is not considered in this paper. Maxima values are compared in this paper rather than time series because 1) extreme values are more influential for risk analysis than low or moderate values, and thus the

comparison of maxima is more relevant in this context, and 2) a time series comparison includes errors in magnitudes and in time, and only the former one is relevant to synthetic hurricanes.

3.1 | Historical hurricanes

A total of 23 historical hurricanes are considered for validation of the models considered in this study. The selection of these 23 hurricanes is determined by the availability of data in H*wind,[28] as gridded hurricane wind field data, which is required in this paper for fitting the Holland *B* parameter, is not provided for events prior to 1998. The selection is also constrained by the requirement that each hurricane must include at least one metocean measurement during the storm. The characteristics of the 23 hurricanes, selected based on these constraints, are listed in Table 2 and their paths are plotted in Fig 1(c). Note that the hurricanes considered here refer to tropical cyclones that reach the intensity of tropical storm or above per the Saffir-Simpson category. It is also noted that, although the paths cover most of the model domain and the hurricane intensities vary from tropical depression to Category 5, most of these hurricanes are low intensity when approaching the nearshore region.

3.2 | Metocean measurements

Metocean measurements from the NDBC (National Data Buoy Center) and the NOS (National Ocean Service) network are considered in this study. All measurements within 250 km from the hurricane trajectories are carefully inspected, and those missing peak values are discarded,

TABLE 2 Number of relevant measurements from offshore buoys and water level stations by hurricane and measurement type

Year	Hurricane	Category*	P_c* (mb)	V_{max}* (m/s)	R_{max}* (km)	Measurement type			
						V	H_s	T_p	η
1999	Dennis	2	963	46	188	10	7	7	4
1999	Floyd	4	921	69	145	16	8	8	14
1999	Irene	2	959	49	216	11	5	5	7
2001	Gabrielle	1	978	36	203	7	3	3	3
2003	Isabel	5	933	72	121	4	3	3	0
2004	Alex	2	970	44	78	17	8	8	8
2004	Charley	3	948	54	82	9	7	7	7
2004	Frances	4	935	64	85	5	1	1	1
2004	Jeanne	3	950	54	68	4	2	2	1
2005	Ophelia	1	976	39	239	33	16	15	9
2005	Wilma	3	929	57	116	4	2	2	0
2006	Beryl	TS	1001	26	91	32	16	16	9
2006	Ernesto	TS	988	31	106	20	12	11	8
2007	Gabrielle	TS	1004	26	120	13	7	7	4
2007	Noel	1	965	39	408	1	6	6	0
2008	Fay	TS	986	31	145	8	6	6	3
2008	Hanna	1	978	39	149	17	23	23	7
2009	Bill	3	948	54	61	1	1	1	0
2009	Danny	TS	1005	26	215	1	1	1	0
2010	Earl	4	931	64	118	14	10	10	5
2011	Irene	3	942	54	249	35	23	23	11
2012	Beryl	TS	993	31	76	12	13	13	3
2012	Sandy	3	944	51	281	17	11	11	3
Total						291	191	189	107

*Characteristics of the hurricane when its trajectory is within the region plotted in Figure 1(a), where P_c represents the minimum recorded value, V_{max} and R_{max} represent the maximum recorded values, and V_{max} is provided here as the 1-min averaged wind speed at an elevation of 10 m.

resulting in measurements from a set of 107 buoys and water level stations during hurricanes, see Figure 1(c). It is worth noting that a potential bias is introduced during this process since missing data is more likely to happen during intense seastates.

The number of relevant measurements recorded for each of the 23 hurricanes and their associated water depths are listed in Tables 2 and 3, respectively. The measurements of storm surge, which are made by water level stations not buoys, are only recorded along the coastline, and no wave measurements, which are made by buoys, are collocated with storm surge measurements. Metocean measurements are recorded at various intervals, ranging from five minutes to one hour, and measurements of wind speed are averaged over a period of either two minutes or eight minutes and recorded at various elevations, varying from 1 m to 50 m. When comparing with model predictions, all measurements are converted to 1-hour intervals, and wind speeds are converted to values at 10 m elevation, using the logarithmic law profile.[47]

3.3 | Performance of metocean prediction models

The prediction performance of the WW3 model is compared with that of the CFSR/Mike 21 model (i.e., the Mike 21 model using CFSR as the meteorological forcing) in Table 4 and in Figures 2 and 3 for 155 measurements of H_s and 153 measurements of T_p. These measurements do not match exactly with those in Table 2 because some of the measurements in shallow water areas are not included in the WW3 model domain. It is important to note that the WW3 model is a global-scale model, while the CFSR/Mike 21 model is a regional model with no waves propagating from outside the domain boundaries. As mentioned earlier, predictions of the WW3 model are provided in 3-hour intervals, and the predictions of the CFSR/Mike 21 model are compared with measurements at the same time instances as the WW3 model. The results indicate that both the CFSR/Mike 21 and WW3 models show a bias, tending to underestimate H_s. The parameters $\sigma_{\varepsilon_{H_s}}$ and $\sigma_{\varepsilon_{T_p}}$ for the WW3 model are 15% higher and 5% lower than those for the CFSR/Mike 21 model, respectively.

A total of 155 measurements of the logarithmic error of H_s are shown in Figure 2. The figure shows that the CFSR/Mike 21 model performs notably better than the WW3 model for measurements of H_s in shallow water, where the WW3 model significantly underestimates H_s in many cases. One explanation for this is that the simulation of H_s in the CFSR/Mike 21 model is coupled with the simulation of storm surge, which allows the water depth to increase and, in turn, allows higher H_s predictions than WW3, which does not include coupling with storm surge. In Figure 3, the logarithmic error of T_p is plotted in terms of H_s measured at the same time and location. The error is plotted in terms of H_s instead of T_p because, in risk analysis, it is common to model T_p conditioned on H_s, so it is useful to observe in Figure 3 that, at high H_s, the prediction error

TABLE 3 Number of relevant measurements from offshore buoys and water level stations by water depth and measurement type

Category	Depth	Number of buoys or stations	Measurement type			
			V	H_s	T_p	η
Shallow	$d \leq 20$ m	69	184	53	53	107
Medium	20 m < $d \leq 60$ m	20	62	74	72	0
Deep	60 m < $d \leq 1000$ m	13	27	42	42	0
Very deep	$d > 1000$ m	5	18	22	22	0

TABLE 4 The prediction performance of the WW3 and CFSR/Mike 21 models.

	$\bar{\varepsilon}_{H_s}$	$\sigma_{\varepsilon_{H_s}}$	$\bar{\varepsilon}_{T_p}$	$\sigma_{\varepsilon_{T_p}}$
WW3	-0.18	0.23	-0.04	0.20
CFSR/Mike 21	-0.12	0.20	0.02	0.21

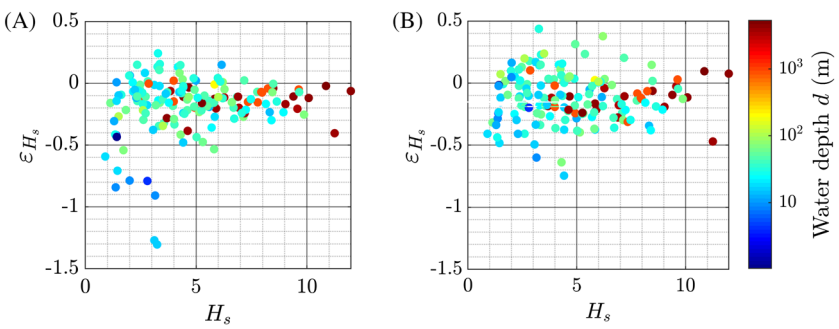

FIGURE 2 The logarithmic error of H_s for the (a) WW3 and (b) CFSR/Mike 21 models

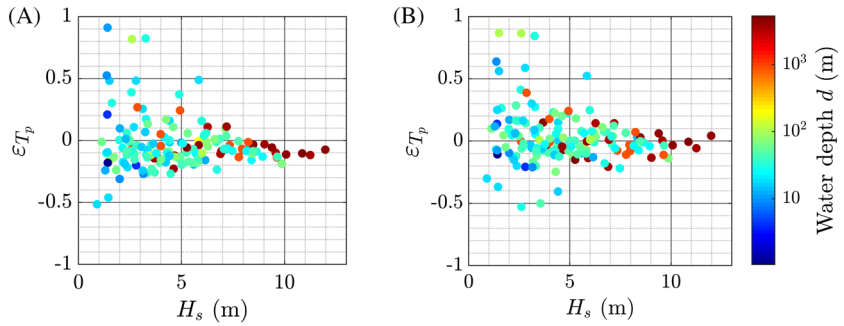

FIGURE 3 The logarithmic error of T_p for the (a) WW3 and (b) CFSR/Mike 21 models

on T_p is low. Overall, for the conditions considered here, the CFSR/Mike 21 model implemented by the authors shows comparable performance with that of WW3, and the remainder of the results in this paper will be based on the Mike 21 model.

4 | IMPACT OF THE METEOROLOGICAL FORCING ON THE MODEL PERFORMANCE

The modeling of hurricane conditions for assessing risk is usually based on a catalog of synthetic hurricanes because of the relatively short duration of the historical record of hurricanes. For synthetic hurricanes, a reanalysis of meteorological conditions, such as CFSR, is not available and so a common approach is to use an empirical model such as the Holland model to estimate meteorological conditions based on a set of parameters describing the hurricane. The Holland model influences metocean predictions compared with reanalysis data in two ways: (1) the simplified shape for the hurricane wind and pressure profiles and (2) the absence of an estimate of meteorological conditions surrounding the hurricane. Three meteorological models (see Table 1) are considered in this section as input to the Mike 21 model to evaluate the impact of the meteorological forcing on metocean predictions, especially to assess the performance of the Holland model without a surrounding wind field, since these conditions are commonly used in assessing risk.

The prediction performance for these three models is summarized in Table 5. The data in this table is slightly different than that in the previous section because of the difference in time intervals for comparing the maximum values (i.e., a 3-hour interval when compared with WW3 in the previous section and a 1-hour interval in this section). The values of $\sigma_{\varepsilon_\eta}$ are the largest among the four measurements for all three models, however, the absolute values of the logarithmic error for storm surge are relatively low (~0.3 m) due to the low values of the measurements. The Hybrid/Mike 21 model shows similar values of σ_{ε_x} (defined in Eq. 8) compared with the CFSR/Mike 21 model, indicating that the simplified hurricane model yields a similar performance as the CFSR reanalysis data. It is important to note that the CFSR data used here does not represent the cutting-edge meteorological forcing due to its limitation in characterizing hurricanes.[15] As such, one can speculate that a precise hurricane reanalysis would outperform the Holland model. Nevertheless, the CFSR results are a useful reference for interpreting the accuracy of the Holland model in characterizing hurricane effects. Compared with the Holland/Mike 21 model, the values of σ_{ε_x} are noticeably lower for the Hybrid/Mike 21 model, indicating that the absence of the meteorological forcing surrounding hurricanes has a significant impact on the metocean responses.

For a closer look at the impact of the meteorological forcing, a total of 291 comparisons between predictions and measurements of V are shown in Figure 4 in terms of the normalized distance r/R_{max}, where r is the distance from hurricane eye and R_{max} is the radius of maximum wind speed of the hurricane. The figure shows that the Holland model performs better than the CFSR model for wind speeds over 20 m/s, while, for wind speeds less than 20 m/s, the Holland model tends to overestimate the wind speed within ~$2R_{max}$ and underestimate the wind speed outside ~$3R_{max}$. The better performance of the Holland model for high wind speeds reflects the limitation of the mesoscale meteorological model, such as CFSR, in modeling hurricane activities. It is also important to note that the measurements here are susceptible to the uncertainties induced by the boundary layer model and averaging time, and for the Holland model, the parameters estimated from the H*wind database are influenced by the factor used to convert from the one-minute maximum wind to mean wind speed. A total of 105 pairs of ε_{H_s} and ε_V, corresponding to all measurements from buoys measuring both V and H_s, are plotted in Figure 5, for all three metocean models. Even though the maxima of V and H_s might not occur concurrently, a significant correlation is still apparent, showing that an underestimation of V is correlated with an underestimation of H_s and vice versa. The correlation coefficient for V and H_s for the Holland/Mike 21 model is 0.72, and, for the CFSR/Mike 21 and Hybrid/Mike 21 models,

TABLE 5 The prediction performance of the Mike 21 model using the CFSR, Holland and Hybrid meteorological forcing

	σ_{ε_V}	$\sigma_{\varepsilon_{H_s}}$	$\sigma_{\varepsilon_{T_p}}$	$\sigma_{\varepsilon_\eta}$
CFSR	0.24	0.22	0.19	0.33
Hybrid	0.23	0.23	0.18	0.34
Holland	0.36	0.31	0.24	0.38

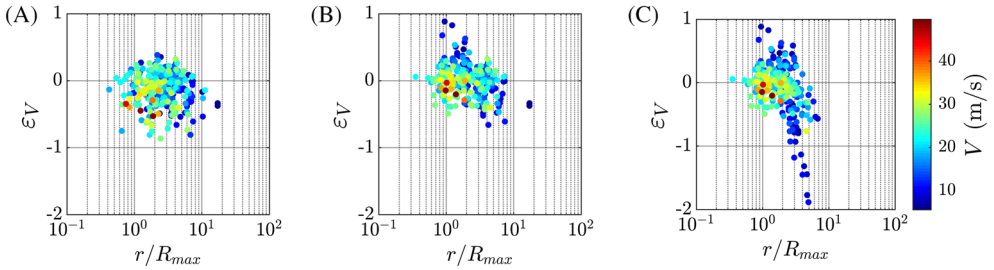

FIGURE 4 The logarithmic error of V for the (a) CFSR/Mike 21, (b) Hybrid/Mike 21, and (c) Holland/Mike 21 models

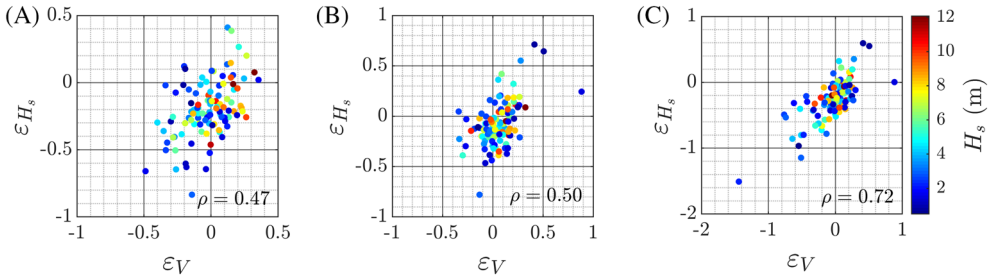

FIGURE 5 The correlation of the logarithmic error of H_s and V for the (a) CFSR/Mike 21, (b) Hybrid/Mike 21, and (c) Holland/Mike 21 models

it is ~0.50. It is important to note that if measurements with wind speed lower than 20 m/s are excluded, the correlation coefficient is ~0.50 for all three models, and the values of σ_{ε_x} for the Holland/Mike 21 model decrease to 0.17, 0.25, 0.23, and 0.33 for V, H_s, T_p, and η, respectively. As such, the high correlation and uncertainty of the Holland/Mike 21 model are mainly caused by the high prediction error for low wind speeds.

In summary, the empirical Holland model shows a similar performance in characterizing hurricanes compared with the CFSR reanalysis, and the inclusion of meteorological conditions surrounding the hurricane is found to significantly improve the performance of the metocean model. However, the negative impact of not including meteorological conditions surrounding a hurricane is effectively diminished by excluding prediction results corresponding to low wind speeds. This makes sense as measurements of V, H_s, T_p, and η during low wind speeds are influenced significantly by conditions outside of the hurricane wind field, while, for high wind speeds, the measurements are dominated by conditions within the hurricane wind field.

5 | UNCERTAINTY QUANTIFICATION AND ITS IMPACT ON ASSESSING RISK

In this section, the results of the Holland/Mike 21 model (i.e., the Mike 21 model using the Holland model for the meteorological forcing) are analyzed to estimate and correct for biases and to quantify uncertainties in simulation results for the 23 historical hurricanes and the corresponding measurements. Following this, a numerical example is provided to demonstrate the impact of prediction uncertainty on the assessment of risk.

5.1 | Bias and uncertainty quantification

Figure 6 shows the logarithmic errors of the Holland/Mike 21 model versus the magnitude of the prediction value. For all measurement types, the standard deviation of the error is higher for low prediction values and tends to stabilize at higher prediction values. As such, lower bounds of $V_{\min}$ = 20 m/s, $H_{s,\min}$ = 2 m, and $\eta_{\min}$ = 1 m are applied in the uncertainty quantification presented here, because, above these lower bounds, the logarithmic error is reasonably stable. Risk analysis is generally more concerned with high values rather than low values, so quantifying the uncertainty in a way that is more representative of high values is reasonable. Note that the lower bound of 20 m/s applied on $\widehat{V}$ is consistent with the threshold discussed in Section 4, above which the prediction performance using the Holland model is comparable with using reanalysis meteorological forcing. Lower bounds of $\widehat{H}_s$ and $\widehat{\eta}$ are chosen here as independent of V, because many of those measurements are not collocated. No lower bound is applied to $\widehat{T}_p$, but only those values corresponding to $\widehat{H}_s \geq H_{s,min}$ are considered.

Linear regression analyses are conducted for the logarithmic error as a function of the prediction value to check for prediction biases for the four measurement types. The analyses indicate that the hypothesis of a zero slope for the relationship of logarithmic error versus prediction for V and η passes a T-test at a significance level of 5%. Thus, for V and η, only the mean logarithmic error is subtracted from the predictions to correct the biases in these two predictions. A Kolmogorov–Smirnov test is conducted on the bias-corrected predictions, and all pass at a 5% significance

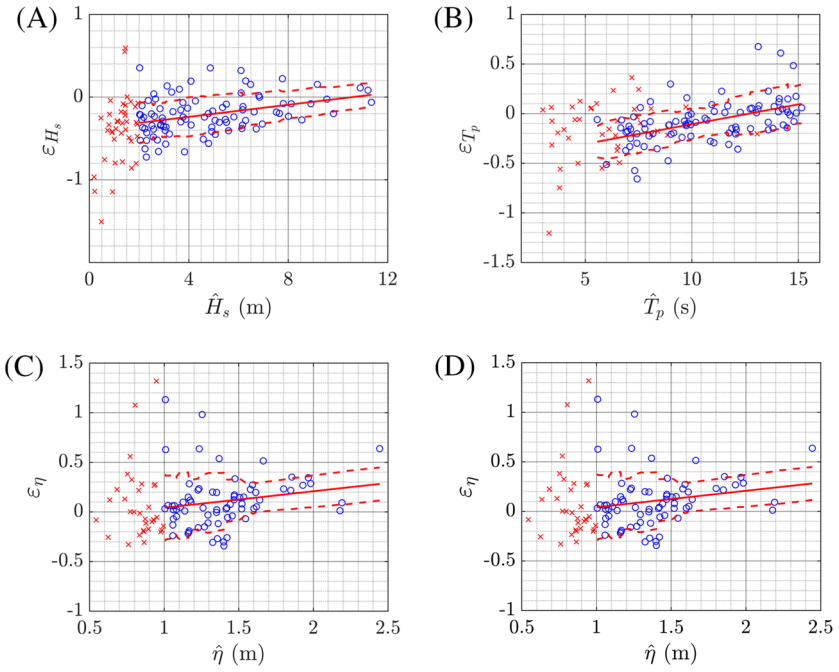

FIGURE 6 Bias and uncertainty quantification for (a) $\widehat{V}$, (b) $\widehat{H}_s$, (c) $\widehat{T}_p$ and (d) $\widehat{\eta}$, with red crosses indicating low values of data that are excluded from the regression analyses, blue circles indicating data included in the regression analyses, red solid lines indicating the results of the linear regression analyses, and red dashed lines indicating the moving standard deviation with a window size of 30 adjacent data

level, suggesting that it is reasonable to use a normal distribution to model the logarithmic prediction uncertainties in V, H_s, T_p, and η. As such, the following equations are suggested here for modeling prediction uncertainties,

$$V_c = \hat{V}\, e^{N-0.055,0.17^2} \tag{9}$$

$$H_{s,c} = \hat{H}_s \cdot e^{N-0.036\hat{H}_s+0.38,0.22^2} \tag{10}$$

$$T_{p,c} = \hat{T}_p \cdot e^{N-0.040\hat{T}_p+0.51,0.18^2} \tag{11}$$

$$\eta_c = \hat{\eta}\, e^{N-0.11,0.27^2} \tag{12}$$

where $\widehat{V}$, $\widehat{H}_s$, $\widehat{T}_p$, and $\widehat{\eta}$ are prediction results from the Holland/Mike 21 model without biases corrected, V_c, $H_{s,c}$, $T_{p,c}$, and η_c are prediction results including bias corrections and uncertainty, and $N(\mu, \sigma^2)$ is a normal random variable with mean μ and variance σ^2. Note that, linear regression analyses are also conducted for ε_V as a function of r/R_{max}, and for ε_{H_s} and ε_{T_p} as a function of water depth, but none of these analyses resulted in biases that passed a T-test at a significance level of 5%.

The correlation coefficients of the paired logarithmic errors after bias correction are provided in Table 6. The results show a significant correlation between ε_V and ε_{H_s} and between ε_{H_s} and ε_{T_p} at a significance level of 5%, while the correlation between ε_V and ε_{T_p} and between ε_V and ε_η is not significant at a significance level of 5%. It is noted that correlations between ε_{H_s}, ε_{T_p} and ε_η are not available, because wave characteristics and storm surge are never measured at the same location for the measurements considered here.

TABLE 6 Correlation coefficients of the logarithmic error for the Holland/Mike 21 model

ε_V	**0.69**	**-0.05**	**-0.03**
	ε_{H_s}	0.26	-
		ε_{T_p}	-
Sym.			ε_η

5.2 | Numerical example

A numerical example is provided here to illustrate the importance of considering uncertainty in the assessment of offshore hurricane risk. The example considers two sites: one located off the coast of South Carolina (SC) and one off the coast of Massachusetts (MA), with water depths of ~16 m and ~50 m, and with distances to the shore of ~30 km and ~60 km, respectively. Both sites are locations where the development of offshore wind farms has been proposed.

This example follows a similar approach to that by Valamanesh et al.[29] and uses a stochastic hurricane catalog developed by Liu[20] to consider 100,000 years of potential hurricane activity. Such a catalog aims to provide more accurate long-term predictions of hurricane wind, since rare synthetic hurricanes can be constructed using hurricane parameters with relatively high and statistically confident probabilities.[48] However, this approach also introduces uncertainties from storm statistics, and these uncertainties are not considered in this paper. Hurricanes that pass within 250 km from these two sites are selected from the catalog, resulting in an arrival rate v of 1.69 year^{-1} for SC and 1.29 year^{-1} for MA. The arrival rates calculated in this paper are slightly higher than those in Valamanesh et al.[29] since a new version of the catalog, based on a database of historical hurricanes with a longer period, is used here. For each site, 1,000 hurricanes are randomly picked from the set of storms passing within 250 km and are analyzed using the Holland/Mike 21 model.

For each of the 1,000 hurricanes at each of the two sites, the maximum wind speed V_{max} and the significant wave height $H_{s,max}$ are extracted from the Holland/Mike 21 model and plotted in Figure 7. The black dots in this figure correspond to data that has been corrected for bias but does not include uncertainty (i.e., substituting $\sigma^2 = 0$ in Eqs. 9 and 10). The Inverse First Order Reliability Method (IFORM)[49] is applied to these results to determine combinations of V and H_s at a mean recurrence period (MRP) of 50 years. In this method, the original data is transformed into uncorrelated random variables u_1 and u_2, each with a marginal standard normal distribution. Combinations of u_1 and u_2 with radial distance β relative to $u_1 = u_2 = 0$ are related to an MRP by $\beta = \Phi^{-1}\left(1 - \frac{1}{v \cdot \text{MRP}}\right)$, where v is the annual arrival rate of hurricanes and Φ^{-1} is the inverse of the cumulative standard normal distribution. An environmental contour associated with the same MRP is obtained by transforming this circle back to the original data space. In this paper, the Rosenblatt transformation[50] is used to transform the original data to uncorrelated standard normal data and the Generalized Extreme Value (GEV) distribution is used to model the distributions of V_{max} and $H_{s,max}$ conditioned on V_{max}. Environmental contours corresponding to an MRP of 50 years are plotted in Figure 7 as green lines.

To consider the effect of uncertainty, 100 realizations of V_{max} and $H_{s,max}$ are sampled for each of the 1,000 hurricanes at each of the two sites using the normal distributions indicated by Eqs. 9 and 10, and the corresponding 50-year environmental contours are shown in Figure 7, with semi-transparent red lines indicating realizations with correlated prediction uncertainties (based on the correlation coefficient in Table 6), and semi-transparent blue lines indicating realizations with uncorrelated prediction uncertainties. The median of the 100 realizations is determined for V and H_s respectively for each pair of u_1 and u_2, shown as a solid red line for correlated uncertainties and as a solid blue line for uncorrelated uncertainties. For both the SC and MA sites, the 50-year environmental contour with uncorrelated uncertainty is larger than the contour without uncertainty. This is not surprising because the 50-year value becomes more extreme as the variance increases. In particular, the independent maximum values of V and H_s for the median 50-year environmental contour increase by ~3 m/s and ~1 m, respectively. Considering the correlation of the uncertainty changes the shape of the median 50-year environmental contour compared with the median 50-year contour without correlation of uncertainty, with the contour with correlation becoming longer along its principal axis and shorter along its secondary axis. The difference is determined by the scale of the covariance of V and H_s relative to the uncertainty. If the uncertainty is relatively large, the contour will be reshaped significantly when the correlation of uncertainty is included. In this example, the uncertainty is relatively small and so the upper right tip of the median 50-year environmental contour changes negligibly when the correlation is included.

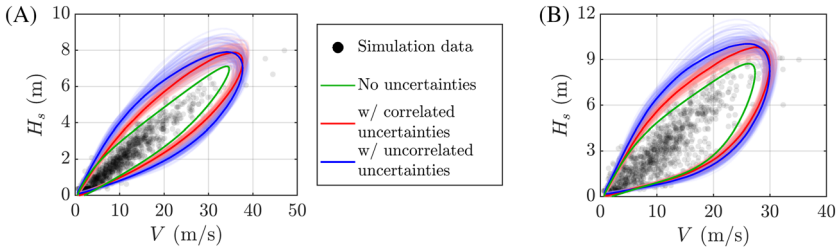

FIGURE 7 Combinations of V and H_s with a 50-year mean recurrence period for the (a) SC and (b) MA sites. Black dots are bias-corrected data from a total of 1,000 numerical simulations of hurricanes. Green lines indicate the corresponding environmental contours. Red and blue lines indicate the contours with correlated and uncorrelated uncertainties respectively, with semi-transparent lines indicating 100 specific realizations and solid lines indicating the median of these realizations

6 | CONCLUSION

Three metocean models are presented in this paper for the U.S. Atlantic coast and the results are validated with (1) measurements of sustained wind speed V, significant wave height H_s, peak spectral period T_p, and storm surge η during 23 historical hurricanes from 1999 to 2012 and (2) hindcast results from the WaveWatch III model. The seastates for the three metocean models are predicted by a numerical model implemented in the commercial software Mike 21, and the meteorological conditions (i.e., the wind and pressure fields) are defined by three combinations of the models within and surrounding the hurricanes. The first uses reanalysis data from CFSR within and surrounding the hurricane, the second uses predictions from the empirical Holland model within the hurricane and CFSR data surrounding the hurricane, and the third uses predictions from the Holland model within the hurricane and wind-free conditions surrounding the hurricane. The first two models show a similar prediction performance, indicating a similar performance of the Holland model in characterizing hurricanes compared with the CFSR reanalysis, which, as mentioned earlier, has important limitations in characterizing important features of hurricane wind fields.[15] The performance of the model is found to be significantly worse when the wind field surrounding the hurricanes is not modeled, however, this negative impact is diminished if predictions during low wind speeds (less than 20 m/s) are excluded from the prediction set. Since risk is influenced more by high wind speeds than by low wind speeds, these results suggest that a metocean model, which considers the Holland model within the hurricane and wind-free conditions surrounding the hurricane for its meteorological forcing, can be reasonably used to assess hurricane risk. Uncertainty is quantified for this model, and the impact of including uncertainty in model predictions and of including correlation of uncertainty in model predictions is demonstrated for a numerical example at two sites along the Atlantic coast. For both sites, including uncertainty is found to increase the size of the 50-year environmental contour of V and H_s compared with a contour without uncertainty, while including correlation for uncertainties is found to change the shape of the contour (the principal axis becomes longer while the secondary axis becomes shorter) compared with a contour with uncorrelated uncertainty, though the upper right tip of the contour changes negligibly.

ACKNOWLEDGEMENT

This material is based upon work supported by the National Science Foundation under grant nos. CMMI-1234560 and CMMI-1552559, the Massachusetts Clean Energy Center, and Northeastern University. Any opinions, findings, and conclusions expressed in this material are those of the authors and do not necessarily reflect the views of the National Science Foundation or other sponsors.

CONFLICT OF INTEREST

The authors declare that they have no conflict of interest.

ORCID

Chi Qiao https://orcid.org/0000-0002-7566-8633

REFERENCES

1. Kim E, Manuel L. A framework for hurricane risk assessment of offshore wind farms. ASME 2012 31st International Conference on Ocean, Offshore and Arctic Engineering; 2012.
2. Hallowell ST, Myers AT, Arwade SR, et al. Hurricane risk assessment of offshore wind turbines. *Renew Energy*. 2018;125:234-249.
3. Mardfekri M, Gardoni P. Multi-hazard reliability assessment of offshore wind turbines. *Wind Energy*. 2015;18(8):1433-1450.
4. Dietrich JC, Zijlema M, Westerink JJ, et al. Modeling hurricane waves and storm surge using integrally-coupled, scalable computations. *Coast Eng*. 2011;58(1):45-65.
5. Kim E, Manuel L. Coupled Atmosphere-Wave-Ocean Modeling to Characterize Hurricane Load Cases for Offshore Wind Turbines. In: *51st AIAA Aerospace Sciences Meeting including the New Horizons Forum and Aerospace Exposition*. American Institute of Aeronautics and Astronautics; 2013.
6. Hanson JL, Tracy BA, Tolman HL, Scott RD. Pacific Hindcast Performance of Three Numerical Wave Models. *J Atmos Oceanic Tech*. 2009;26(8):1614-1633.
7. Holland GJ. An Analytic Model of the Wind and Pressure Profiles in Hurricanes. *Mon Weather Rev*. 1980;108(8):1212-1218.
8. Cardone V, Cox A. Tropical cyclone wind field forcing for surge models: Critical issues and sensitivities. *Nat Hazards*. 2009;51(1):29-47.
9. Resio DT, Irish JL, Westerink JJ, Powell NJ. The effect of uncertainty on estimates of hurricane surge hazards. *Nat Hazards*. 2013;66(3):1443-1459.
10. Saha S, Moorthi S, Pan HL, et al. The Ncep Climate Forecast System Reanalysis. *B Am Meteorol Soc*. 2010;91(8):1015-1057.
11. van Verseveld HCW, van Dongeren AR, Plant NG, Jäger WS, den Heijer C. Modelling multi-hazard hurricane damages on an urbanized coast with a Bayesian Network approach. *Coast Eng*. 2015;103:1-14.
12. Saha S, Nadiga S, Thiaw C, et al. The NCEP Climate Forecast System. *J Climate*. 2006;19(15):3483-3517.

13. Saha S, Moorthi S, Pan H-L, et al. NCEP Climate Forecast System Reanalysis (CFSR) Selected Hourly Time-Series Products, January 1979 to December 2010. In. Boulder, CO: Research Data Archive at the National Center for Atmospheric Research, Computational and Information Systems Laboratory; 2010.
14. Saha S, Moorthi S, Wu X, et al. NCEP Climate Forecast System Version 2 (CFSv2) Selected Hourly Time-Series Products. In. Boulder, CO: Research Data Archive at the National Center for Atmospheric Research, Computational and Information Systems Laboratory; 2011.
15. Cox AT, Cardone VJ, Swail VR. On the use of the climate forecast system reanalysis wind forcing in ocean response modeling. Paper presented at: Proceedings, 12th int. Workshop wave, hindcasting, forecasting, Hawaii, USA; 2011.
16. Skamarock WC, Klemp JB, Dudhia J, et al. *A description of the advanced research WRF version 2*. DTIC Document; 2005.
17. Cardone VJ, Cox AT, Forristall GZ. Hindcast of winds, waves and currents in northern Gulf of Mexico in Hurricanes Katrina (2005) and Rita (2005). Paper presented at: Offshore Technology Conference; 2007.
18. Swail V, Cardone V, Ferguson M, et al. The MSC50 wind and wave reanalysis. Paper presented at: Proceedings of the 9th International Workshop on Wave Hindcasting and Forecasting; 2006.
19. Wang Y. *Studies on hazard characterization for performance-based structural design*, Texas A&M University; 2010.
20. Liu F. *Projections of Future US Design Wind Speeds Due to Climate Change for Estimating Hurricane Losses*, Clemson University; 2014.
21. Wei K, Arwade SR, Myers AT, Valamanesh V, Pang W. Effect of wind and wave directionality on the structural performance of non-operational offshore wind turbines supported by jackets during hurricanes. *Wind Energy*. 2016;20(2):289-303.
22. Vickery PJ, Wadhera D, Powell MD, Chen YZ. A Hurricane Boundary Layer and Wind Field Model for Use in Engineering Applications. *J Appl Meteorol Clim*. 2009;48(2):381-405.
23. Georgiou PN, Davenport AG, Vickery BJ. Design Wind Speeds in Regions Dominated by Tropical Cyclones. *J Wind Eng Ind Aerod*. 1983;13(1-3):139-152.
24. Xie L, Bao S, Pietrafesa LJ, Foley K, Fuentes M. A Real-Time Hurricane Surface Wind Forecasting Model: Formulation and Verification. *Mon Weather Rev*. 2006;134(5):1355-1370.
25. Hu K, Chen Q, Kimball SK. Consistency in hurricane surface wind forecasting: an improved parametric model. *Nat Hazards*. 2012;61(3):1029-1050.
26. Gao J. *On the Surface Wind Stress for Storm Surge Modeling*, University of North Carolina at Chapel Hill; 2018.
27. Knapp KR, Kruk MC, Levinson DH, Diamond HJ, Neumann CJ. The International Best Track Archive for Climate Stewardship (IBTrACS). *B Am Meteorol Soc*. 2010;91(3):363-376.
28. Powell MD, Houston SH, Reinhold TA. Hurricane Andrew's landfall in south Florida. Part I: standardizing measurements for documentation of surface wind fields. *Weather Forecast*. 1996;11(3):304-328.
29. Valamanesh V, Myers AT, Arwade SR, Hajjar JF, Hines E, Pang W. Wind-wave prediction equations for probabilistic offshore hurricane hazard analysis. *Nat Hazards*. 2016;83(1):541-562.
30. Vickery PJ, Wadhera D. Statistical Models of Holland Pressure Profile Parameter and Radius to Maximum Winds of Hurricanes from Flight-Level Pressure and H*Wind Data. *J Appl Meteorol Clim*. 2008;47(10):2497-2517.
31. Harper B, Kepert J, Ginger J. Guidelines for converting between different wind averaging periods in tropical cyclone conditions. *World Meteorological Organization*. 2008.
32. Tanemoto J, Ishihara T. Prediction of tropical cyclone induced wind field by using mesoscale model and JMA best track. Paper presented at: Proceedings of 8th Asia Pacific conference on Wind Engineering; 2013.
33. Ataei N, Padgett JE. Fragility surrogate models for coastal bridges in hurricane prone zones. *Eng Struct*. 2015;103:203-213.
34. DHI. *MIKE21-FM HD Scientific Documentary*. Denmark: DHI Water and Environment; 2014.
35. DHI. *MIKE21 SW Scientific Documentary*. Denmark: DHI Water and Environment; 2014.
36. Westerink JJ, Luettich RA, Feyen JC, et al. A basin- to channel-scale unstructured grid hurricane storm surge model applied to southern Louisiana. *Mon Weather Rev*. 2008;136(3):833-864.
37. Chawla A, Spindler DM, Tolman HL. Validation of a thirty year wave hindcast using the Climate Forecast System Reanalysis winds. *Ocean Model*. 2013;70:189-206.
38. Amante C, Eakins BW. ETOPO1 1 Arc-Minute Global Relief Model: Procedures, Data Sources and Analysis. *NOAA Technical Memorandum NESDIS NGDC-24 National Geophysical Data Center, NOAA*. 2009.
39. NOAA. U.S. Coastal Relief Model. In:2008.
40. Stewart J, Callaghan D, Nielsen P. *Tropical cyclone ROGER strom surge assessment*. University of Qweensland; 2010.
41. Wu J. The sea surface is aerodynamically rough even under light winds. *Bound-Lay Meteorol*. 1994;69(1-2):149-158.
42. DHI. *MIKE 21 Toolbox -Global Tide Model -Tide prediction*. Denmark: DHI Water and Environment; 2014.
43. Battjes J, Janssen J. Energy loss and set-up due to breaking of random waves. *Coast Eng Proc*. 1978;1(16):32.
44. Weber N. Bottom friction for wind sea and swell in extreme depth-limited situations. *J Phys Oceanogr*. 1991;21(1):149-172.
45. Bidlot J, Janssen P, Abdalla S, Hersbach H. A revised formulation of ocean wave dissipation and its model impact. 2007.
46. Park H, Cox DT. Empirical wave run-up formula for wave, storm surge and berm width. *Coast Eng*. 2016;115:67-78.
47. Simiu E. *Design of Buildings for Wind*. Hoboken, New Jersey: John Wiley & Sons, Inc.; 2011.
48. 19901-1 I. Petroleum and natural gas industries-specific requirements for offshore structures-Part 1: metocean design and operating conditions. 2015.

49. Winterstein SR, Ude TC, Cornell CA, Bjerager P, Haver S. Environmental parameters for extreme response: Inverse FORM with omission factors. *Proceedings of the ICOSSAR-93, Innsbruck, Austria*. 1993:551-557.

50. Rosenblatt M. Remarks on a multivariate transformation. *Ann Math Stat*. 1952;23(3):470-472.

How to cite this article: Qiao C, Myers AT, Arwade SR. Validation and uncertainty quantification of metocean models for assessing hurricane risk. *Wind Energy*. 2020;23:220–234. https://doi.org/10.1002/we.2424